Author/s:
Duc, D;Stoddart, PR;McArthur, SL;Kapsa, RMI;Quigley, AF;Boyd-Moss, M;Moulton, SE

Title:
Fabrication of a Biocompatible Liquid Crystal Graphene Oxide–Gold Nanorods Electro- and Photoactive Interface for Cell Stimulation

Date:
2019-05-09

Citation:
Duc, D., Stoddart, P. R., McArthur, S. L., Kapsa, R. M. I., Quigley, A. F., Boyd-Moss, M. & Moulton, S. E. (2019). Fabrication of a Biocompatible Liquid Crystal Graphene Oxide–Gold Nanorods Electro- and Photoactive Interface for Cell Stimulation. Advanced Healthcare Materials, 8 (9), https://doi.org/10.1002/adhm.201801321.

Persistent Link:
https://hdl.handle.net/11343/285520

Fabrication of a biocompatible liquid crystal graphene oxide-gold nanorods electro- and photoactive interface for cell stimulation

Daniela Duc[1], Paul R. Stoddart[1,2], Sally L. McArthur[1,2], Robert M. I. Kapsa[3,4,5], Anita F. Quigley[3,4,5], Mitchell Boyd-Moss[5,6], and Simon E. Moulton[1,7,*]

[1]ARC Centre of Excellence for Electromaterials Science, Faculty of Science, Engineering and Technology, Swinburne University of Technology, John St, Hawthorn, VIC 3122, Australia.

[2]ARC Training Centre in Biodevices, Swinburne University of Technology, John St, Hawthorn, VIC 3122, Australia.

[3]ARC Centre of Excellence for Electromaterials Science, Intelligent Polymer Research Institute AIIM, University of Wollongong Innovation Campus, Squires Way, North Wollongong, NSW 2500, Australia.

This is the author manuscript accepted for publication and has undergone full peer review but has not been through the copyediting, typesetting, pagination and proofreading process, which may lead to differences between this version and the Version of Record. Please cite this article as doi: 10.1002/adhm.201801321.

[4] Department of Medicine, St Vincent's Hospital, The University of Melbourne, 41 Victoria Parade, Fitzroy, VIC 3065, Australia.

[5] Biofab3D@ACMD, St. Vincent's Hospital, 41 Victoria Parade, Fitzroy, VIC 3065, Australia.

[6] School of Engineering, RMIT University, 124 La Trobe St, Melbourne, VIC 3000, Australia.

[7] Iverson Health Innovation Research Institute, Swinburne University of Technology, John St, Hawthorn, VIC 3122, Australia.

*Corresponding author: smoulton@swin.edu.au

Keywords: Liquid crystal graphene oxide, gold nanorods, electrical stimulation and near-infrared stimulation, neurons.

ABSTRACT

For decades, electrode-tissue interfaces have been pursued to establish electrical stimulation as a reliable means to control neuronal cells behaviour. However, spreading of electrical currents in tissues limits its spatial precision. Thus, optical cues, such as near-infrared (NIR) light, have been explored as alternatives. Presently, NIR stimulation requires higher energy input than electrical methods

despite introduction of light absorbers e.g. gold nanoparticles. As potential solution, NIR and electrical co-stimulation have been proposed but with limited interfaces capable of sustaining this stimulation technique. Here, we constructed a novel electroactive nanocomposite with photoactive properties in the NIR range by EDC/NHS conjugation of liquid crystal graphene oxide (LCGO) to protein-coated gold nanorods (AuNR). The liquid crystal graphene oxide-gold nanorod nanocomposite (LCGO-AuNR) was fabricated into a hydrophilic electrode-coating via drop-casting, making it appropriate for versatile electrode-tissue interface fabrication. UV-Vis spectrophotometry results demonstrated that LCGO-AuNR presented an absorbance peak at 798nm (NIR range). Cyclic voltammetry measurements further confirmed its electroactive capacitive properties. Furthermore, LCGO-AuNR coating supported cell adhesion, proliferation and differentiation of NG108-15 neuronal cells. We anticipate this biocompatible interface, with ideal electrical and optical properties for NIR and electrical co-stimulation, to enable further development of the technique for energy-efficient and precise neuronal cell modulation.

Introduction

Neuronal cell stimulation is an essential technique applied in neuroscience-related technologies for the study and control of neuronal function, development and disorders such as Parkinson's disease.[1],[2],[3] For decades, electrical stimulation has been the method of choice for modulating neuronal behaviour using extrinsic physical cues[4]. This

paved the way for the development of a wide variety of biocompatible and conductive electrode-tissue interfaces. They range from platinum alloys,[5] which are the gold standard today, to more recent developments such as conductive polymers,[6] carbon nanotubes[7] and conductive nanoparticles, for instance silver nanowires or nanocrystalline diamond.[8] With advancements in neuroscience research, it has been understood that precise spatial and temporal control of neuronal stimulation is essential to achieve interfacing down to the single-cell level.[9] Progress in electrode-interface design and materials, for instance *via* microfabrication technology, has increased spatial and temporal precision of electrical stimulation of neuronal tissue.[10] However, remaining limitations such as tissue damage due to high stimulating current[11] and challenges to stimulate cells individually still persist.[9]

Consequently, alternative neuronal cell stimulation techniques are being explored, with optical cell stimulation being one of the prime techniques of interest.[4,12] A range of optical stimulation techniques have been introduced, including optogenetics[12], advanced photoactive materials[13,14] and infrared (IR) neuronal stimulation.[12] IR stimulation has the potential advantages of high spatiotemporal precision and reduced tissue inflammation as contact with foreign materials is not required.[15] A sub-type of IR stimulation called near-infrared (NIR) stimulation uses NIR light to stimulate cells through two-photon-based photothermal effect.[16] Wavelengths in the NIR optical window (650-1450 nm) are attractive for improved light penetration and reduced heating of tissues due to the relatively low tissue absorbance in that range.[17] Despite these advantages,

challenges with high energy input,[18] residual tissue heating[19] and low tissue penetration (millimeter range)[20] remain a concern. As a solution, absorbers such as metallic nanoparticles have been introduced in NIR stimulation creating a technique called nanoparticle-enhanced NIR (NP-NIR) stimulation.[21] Its ability to control neuronal tissue differentiation[22] and to trigger calcium transients or action potentials in neurons has been shown but overall energy efficiency still remains an issue.[21,23]

As a potential solution to these drawbacks of optical and electrical stimulation when used as isolated techniques, combined electrical-optical co-stimulation has been proposed. Duke *et al.* (2009) explored this approach by applying subthreshold electrical stimuli together with IR stimulation to the rat sciatic nerve to trigger an evoked response.[24] The optical threshold was found to decrease by as much as a factor of three in terms of radiant exposure, resulting in less heat deposition in the target tissue.[24] Despite these promising results, co-stimulation approaches remain relatively undeveloped. Considering interfaces capable of mediating NIR stimulation of cells, a variety of effective interfaces have been developed, for instance graphene nanomesh semiconductors by Akhavan *et al.*, 2015, which have shown to modulate human neural stem cells differentiation by photoelectric effect of the interface.[25] The current range of materials and interfaces capable of sustaining such electrical and optical cell co-stimulation are also quite limited in number and in their capabilities.[26] Therefore, significant research in the careful combination of materials for this purpose is indispensably required.

With the aim to manufacture a novel tissue-electrode interface capable of mediating NIR and electrical co-stimulation of neuronal cells effectively, this study investigated a nanocomposite structure formed from two components. The first one is liquid crystal graphene oxide (LCGO) whose properties make it a suitable candidate as an interface for electrical cell stimulation. LCGO is known for its large sheet size which greatly facilitates the fabrication of graphene materials.[27] It possesses highly oxidized basal plane and edge functional groups, including carboxyls,[28] that can be used for further functionalization of the material. Its conductivity can also be modulated based on the extent of reduction.[29] Moreover, it has strong mechanical properties that allow it to withstand the mechanical strains of cell stimulation and have enabled its use in the production of highly flexible electrodes.[29] Its capacity to produce highly wrinkled topographies can potentially improve electrical properties at the electrode-tissue interface.[29] LCGO and its derivatives have further shown high biocompatibility with neuronal tissue and other cell types [29,30] and has shown to improve certain cell behaviours such as cell proliferation.[30] This biocompatibility is further emphasized by its high colloidal stability in water[27] and consequent functionality in aqueous media rather than toxic organic solvents.

The second component of the proposed system is gold nanorods. As mentioned previously, in NP-NIR stimulation, several nanomaterials have been used as absorbers, for instance iron oxide[31] and gold.[21,26,32] Gold nanoparticles have shown high biocompatibility with neuronal cells and can be functionalized for additional biological functions.[32,33] They exhibit localized surface plasmon resonance (LSPR), a phenomenon

whereby electrons at the surface of the nanoparticle oscillate in response to irradiation with light of a specific wavelength.[34] This produces a photothermal effect which can be used to stimulate cells.[23,34] By adjusting the material composition and aspect ratio of the gold nanorods, the LSPR absorption peak can be tuned to specific wavelengths in the NIR range.[34] In addition, the photothermal effect generated is highly localized at the nanoparticle, which creates a steep thermal gradient within a radius of tens of nanometers around the gold nanoparticle. This results in high spatial resolution of the stimulation.[35] Also, high temporal resolution can be achieved as the duration of the photothermal effect is governed by the length of the laser pulse (typically in the range 0.1-10 ms).[23]

In this paper, liquid crystal graphene oxide (LCGO) and protein-coated gold nanorods (AuNR) were conjugated by EDC/NHS chemistry to produce a novel liquid crystal graphene oxide-gold nanorod nanocomposite (LCGO-AuNR) aimed for electrical and NP-NIR co-stimulation of neuronal cells. The novelty LCGO-AuNR does not only lie in its potential capacity of mediating both electrical and NIR stimuli but also in the careful design and combination of LCGO with a strong photothermal converter, AuNR[23] for biological applications. As part of this work, the NIR optical properties and electrical characteristics were evaluated by UV-Vis spectrophotometry and cyclic voltammetry respectively. The morphology and surface properties of LCGO-AuNR films were assessed using scanning electron microscopy (SEM), transmission electron microscopy (TEM), atomic force microscopy (AFM), X-ray photoelectron spectroscopy (XPS) and contact angle

measurements. The biocompatibility of the LCGO-AuNR films was evaluated using the NG108-15 somatic hybridism cell line which models cholinergic neurons and is derived from rat glioma C6 BV-1 and mouse neuroblastoma N18TG-2 cell lines.[36] The adhesion, cytotoxicity, proliferation and differentiation of NG108-15 cells on the LCGO-AuNR platform were investigated.

Results and Discussion

Confirmation of LCGO-AuNR synthesis

FTIR was performed to confirm the EDC/NHS conjugation of LCGO to AuNR, illustrated in Figure1a. As shown in Figure1b, the FTIR spectrum of LCGO presented peaks at 3390 cm^{-1}, 1710 cm^{-1}, 1630 cm^{-1}, 1220 cm^{-1} and 1050 cm^{-1} which were attributed to the O-H bond stretch, C=O in carboxylic acid, C=C, C-O-C and C-O stretch groups respectively.[37,38] The AuNR showed peaks at 3451 cm^{-1}, 2868 cm^{-1}, 1742 cm^{-1}, 1654 cm^{-1}, 1460 cm^{-1} and 1103 cm^{-1} corresponding to N-H/O-H, C-H, C=O, amide I, amide II, C-O groups present in the protein coating of the gold nanorods respectively.[37,39] The success of the EDC/NHS conjugation was confirmed firstly by the presence of characteristic amide-carbonyl (-NH-CO-) stretching (amide I) at 1621 cm^{-1} in LCGO-AuNR.[37,38] Secondly, the disappearance of carboxylic acid stretch (C=O) in LCGO-AuNR at 1710 cm^{-1} indicated that the -COOH group of LCGO were consumed in the conjugation to form the amide linkage (Figure1b *arrow*).[37–39] The appearance of C-H stretch peaks at 2800 cm^{-1} in LCGO-AuNR, resulting from the CH_2 groups of the gold nanorods' protein-coating present in the nanocomposite,

further confirmed the conjugation. The peak at 3229 cm^{-1} in LCGO-AuNR resulted from N-H/O-H stretches. The importance of the conjugation of LCGO to AuNR is to ensure interaction of AuNR with the cell membrane and prevent internalization of AuNR by the cells.[21]

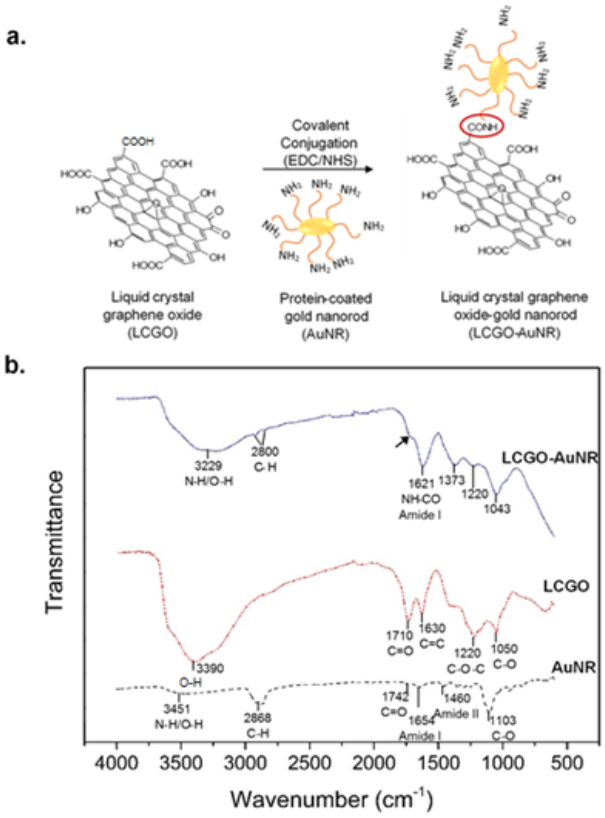

Figure 1 a. Schematic diagram of EDC/NHS conjugation of LCGO and AuNR. The -NH2 group from the protein-coating of the AuNR reacts with the activated -COOH group of the LCGO to form an amide (-CONH-) linkage (encircled). b. FTIR spectra of LCGO-AuNR, LCGO and AuNR (protein-coating) for the wavenumber range of 600-4000 cm^{-1}. The wavenumber and corresponding bonds are indicated for each peak. The arrow indicates the disappearance of the C=O stretch at 1710 cm^{-1} in LCGO-AuNR.

Optical properties of LCGO-AuNR

The UV-Vis spectrum of LCGO (Figure2a) showed a peak at ~230 nm, due to $\pi \rightarrow \pi^*$ transitions of aromatic C=C bonds, and a shoulder at 300 nm, due to $n \rightarrow \pi^*$ transitions of C=O bonds.[38] These are typical of graphene oxide[38]. In the profile of LCGO-AuNR, these two peaks could be observed thus showing the presence of LCGO in the composite. A third peak was observed in the UV-Vis spectrum of LCGO-AuNR at 798nm due to the localized surface plasmon resonance (LSPR) of the AuNR present in the nanocomposite (Figure2a). This further confirmed the EDC/NHS conjugation and showed the photoactivity of LCGO-AuNR nanocomposite in the NIR range.

In effect, the UV-Vis profile of AuNR (Figure2b) presented a maximum longitudinal LSPR peak at 798 nm which showed their photoactive properties in the optical window (650–1450 nm) of the NIR range.[17] A second peak was observed at 523 nm corresponding to the transverse LSPR of the nanorods and, to a minor extent, the LSPR of some nanospheres present (see Supplementary FigureS1). From the UV-Vis spectrum of LCGO-AuNR, we further estimated the mean concentration of LCGO-AuNR suspension produced at 0.27±0.04 mg ml^{-1} (*n=4*). Each fabrication cycle also produced an average of 25±1 ml (*n=3*) of LCGO-AuNR suspension. (Supplementary FigureS2).

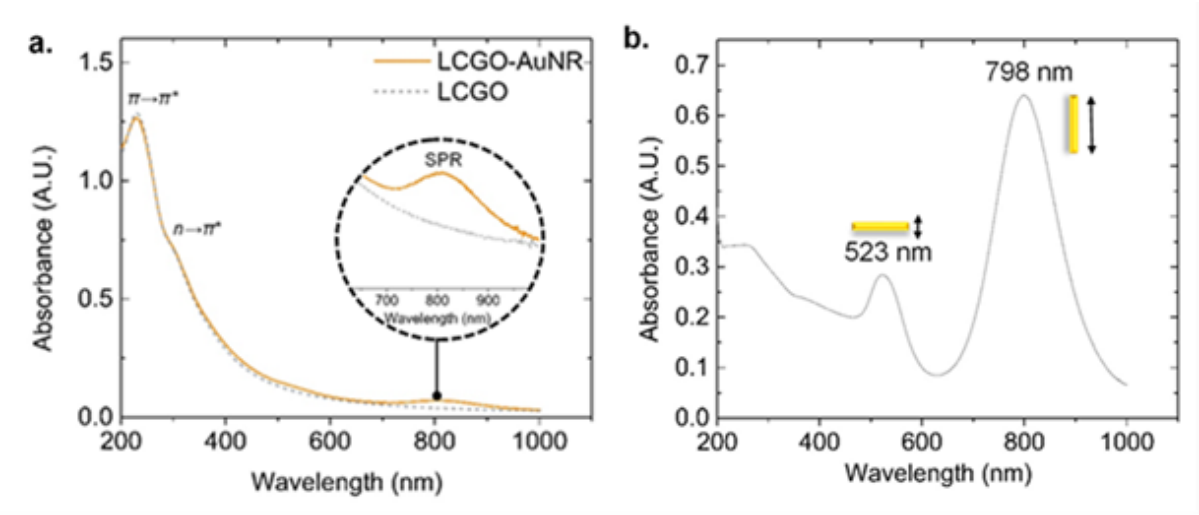

Figure 1 a. UV-Vis spectra of LCGO (0.02 mg ml^{-1}) and LCGO-AuNR (0.02 mg ml^{-1}) for the wavelength range 200–1000 nm. LCGO-AuNR and LCGO showed a peak at ~230 nm ($\pi\rightarrow\pi^*$ transitions) and a shoulder at 300 nm ($n\rightarrow\pi^*$ transitions of C=O bonds). Magnified image shows the presence of an SPR peak at 798 nm in LCGO-AuNR. b. UV-Vis spectrum of protein-coated gold nanorods (AuNR) suspension of 0.039 mg ml^{-1}. The maximum longitudinal LSPR peak and the transverse peak are shown at 798 nm and 523 nm respectively.

Morphology of LCGO-AuNR film

Presence of both gold nanospheres and nanorods was observed on the scanning electron microscopy (SEM) image of the protein-coated gold nanoparticles (Figure3a). The SEM image of LCGO (Figure3b) showed a wrinkled topography, typical of LCGO[40,41], which is formed by thermodynamic requirements and interactions of LCGO with the substrate.[42] This is usually observed in graphene-based materials.[42] As expected, the SEM image of LCGO-AuNR (Figure3c) showed both presence of gold nanoparticles (both nanorods and

nanospheres) and graphene-like wrinkles of LCGO. This wrinkled morphology of LCGO-AuNR is advantageous as it offers an increased surface area for cell stimulation as well as interaction between the cell and the interface.

The density on the LCGO-AuNR film was evaluated at 2.19±0.05 gold nanorods μm^{-2} (*n=3)* which could ensure interaction between the nanorods and the cells. Our measurement of the average area of an NG108-15 cell body at 4h being approximately 100 μm^2 (Figure7b), we deduced that any NG108-15 cell cultured on the single-layer LCGO-AuNR film would be in contact with an average of 219 gold nanorods.

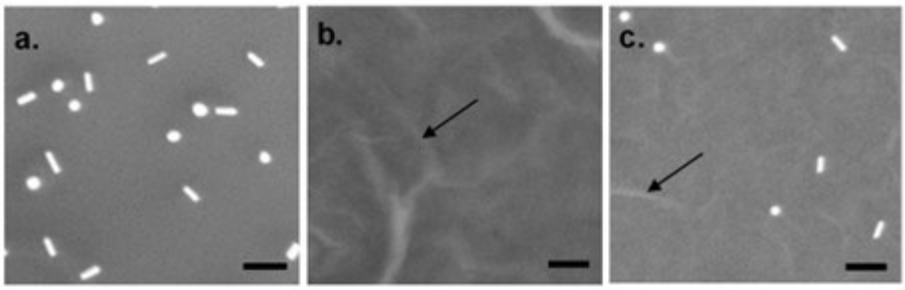

Figure 3 Scanning electron microscopy (SEM) images of a. AuNR b. LCGO and c. LCGO-AuNR films (100000X magnification). SEM image of LCGO-AuNR shows the presence of AuNR (white rods and spheres) and graphene-like wrinkles typical of LCGO (arrow). Scale: 200 nm.

Finer structures of LCGO and LCGO-AuNR were observed *via* transmission electron microscopy (TEM). TEM images of LCGO (Figure4a) presented multi-layered sheets of LCGO with a high level of wrinkles, ripples and some crumples, usually observed in LCGO[41]. The single sheets of LCGO observed were large with a lateral width of more than

1µm (Figure4b). This characteristic makes LCGO an advantageous material for electrode interface fabrication as an important sheet size ensures ease of processibility and coverage[43]. The TEM images of LCGO-AuNR showed presence of both gold nanorods and nanospheres conjugated to LCGO on the multi-layered sheets (Figure4c). Marginally large single sheets of LCGO-AuNR conjugated with nanorods were also observe (Figure4d). This further confirmed the success of the conjugation method used. These LCGO-AuNR films presented a slightly higher degree of wrinkling compared to single sheets of LCGO possibly due to an increase of π-π stacking caused by the loss of some oxygen groups during the conjugation process.[44]

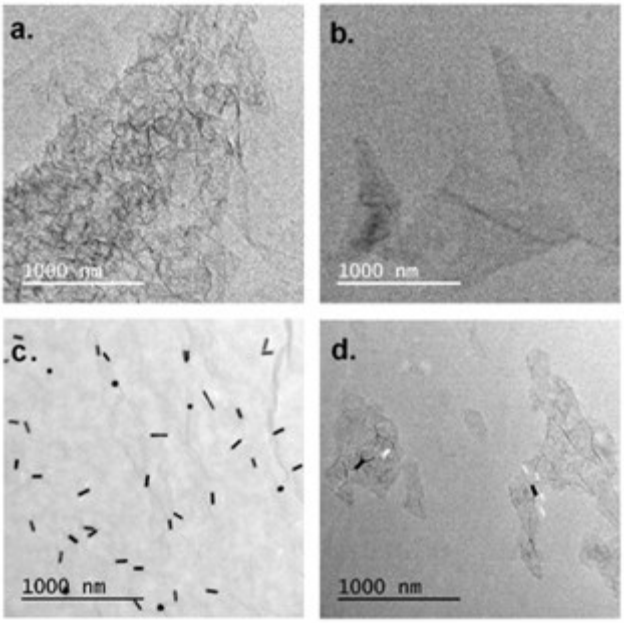

Figure 4 Transmission scanning microscopy (TEM) images of a. multi-layered sheets of LCGO b. single LCGO sheets c. multi-layered sheets of LCGO-AuNR and d. single LCGO-AuNR sheets (7500X magnification). The presence of AuNR were observed on single sheets of LCGO in LCGO-AuNR. Note: white spots are artefacts possibly due to reflection of beam.

Surface Properties of LCGO-AuNR film

The drop-casting method used formed a LCGO-AuNR coating with full substrate coverage of 0.12mg cm^{-2}. The surface roughness of LCGO-AuNR films on air-plasma treated glass (LCGO-AuNR/AP Glass) and on air-plasma treated gold mylar (LCGO-AuNR/AP GM) were quantified by measuring the root mean square roughness, Rq via AFM. The Rq reflects the dispersion of film height distribution from the mean.[45] LCGO-AuNR presented higher surface roughness than the bare substrates (Figure 5b and e). The LCGO-AuNR films presented a nanorough surface with wrinkles, ripples and grooves (Figure5a and d). These were more pronounced in LCGO-AuNR/AP GM with a higher Rq in LCGO-AuNR/AP GM (27±8 nm; *n=3*) than in LCGO-AuNR/AP Glass (15±5 nm; *n=3*) (one-way ANOVA, *p<0.05*; *Tukey HSD; p<0.05*) (Figure5b and e). This is an advantageous feature as surface roughness is an important parameter in neuronal cell adhesion with neuronal cells tending to adhere better to nanorough surfaces.[46] LCGO-AuNR interface (*n=3*) showed a lower surface roughness than LCGO (*n=3*) (ANOVA, *p<0.05*; *Tukey HSD; p<0.05)* on glass but not on gold mylar (one-way ANOVA, *p<0.05*; *Tukey HSD; p>0.05*). Such differences may be explained by dissimilarities in interaction between LCGO-AuNR and the respective substrates due to their different physicochemical nature.

Contact angle measurements showed that LCGO-AuNR films were hydrophilic with contact angles inferior to 90° (Figure5c and f). LCGO-AuNR/AP Glass and LCGO-AuNR/ AP GM

presented statistically similar contact angles of 44±3° (*n=3*) and 43±3° (*n=3*) respectively (one-way ANOVA, *p<0.05*; *Tukey HSD; p>0.05*). These were no different from their LCGO counterparts *(n=3)* (one-way ANOVA, *p<0.05*; *Tukey HSD; p>0.05*). Such similarity could be explained by little differences in expression of oxygen groups between LCGO-AuNR and LCGO[47] and little effect due to the difference in surface roughness observed above. Higher hydrophilicity was observed for AP Glass (31±5°; *n=3*) compared to AP GM (53°±4° *n=3*) (one-way ANOVA, *p<0.05; Tukey HSD; p<0.05*) with air-plasma treatment. This may be explained by different surface densities of hydrophilic groups (namely oxygen groups) on AP Glass and AP GM under the same conditions.

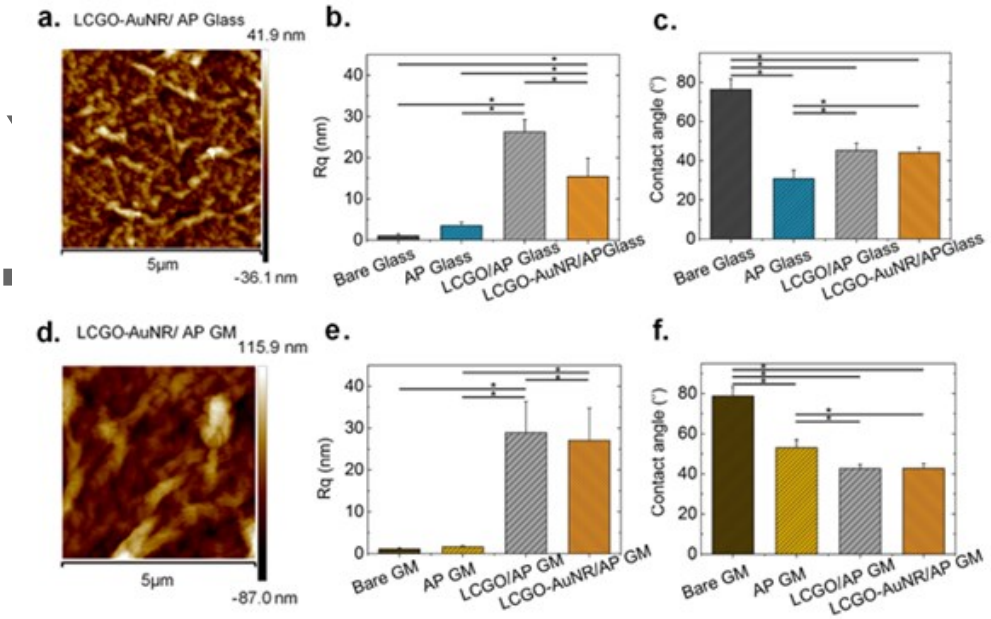

Figure 5 a. Height mode atomic force microscopy (AFM) image of LCGO-AuNR deposited on air-plasma treated glass (LCGO-AuNR/ AP Glass). b. Analysis of surface roughness, quantified in root mean square deviation (Rq) of bare glass *(n=3)*, air-plasma treated glass (AP Glass) *(n=3)*, LCGO deposited on air-plasma treated glass (LCGO/AP Glass) *(n=3)* and LCGO-AuNR/ AP Glass *(n=3)*. c. Contact angle (CA) measurement of bare glass *(n=3)*, AP Glass *(n=3)*, LCGO/AP Glass *(n=3)* and LCGO-AuNR/AP Glass *(n=3)*. d. Height mode AFM image of LCGO-AuNR deposited on air-plasma treated gold mylar (LCGO-AuNR/ AP GM). e. Analysis of surface roughness, in Rq, of bare gold mylar (GM) *(n=3)*, air-plasma treated gold mylar (AP GM) *(n=3)*, LCGO deposited on air-plasma treated gold mylar (LCGO/AP GM) *(n=3)* and LCGO-AuNR/ AP GM *(n=3)*. f. CA measurement of bare GM *(n=3)*, AP GM *(n=3)*, LCGO/AP GM *(n=3)* and LCGO-AuNR/AP GM *(n=3)*. Note: Mean values are represented in Figures 5b, c, e and f. Error bars represent the standard deviation, S.D.

"*" indicates a statistically significant difference of p-value, *p< 0.05* (one-way ANOVA and Tukey HSD post-hoc test).

X-ray photoelectron spectroscopy (XPS) of LCGO-AuNR showed carbon atoms (C) as the major element at 67±2% (*n=3*) followed by oxygen (O) at 28±1% (*n=3*). These percentages were statistically similar to those observed in LCGO (*n=3*) for C and O thus yielding similar carbon to oxygen ratios (*t*-test; *p>0.05*) (see Supplementary Table1 and Supplementary FigureS3). The presence of nitrogen (N) at 2.2±0.3% (*n=3*) and gold (Au) at 0.02±0.01% (*n=3*) atoms in LCGO-AuNR only further confirmed the successful conjugation of AuNR to LCGO. The C1s spectrum of LCGO-AuNR (see Supplementary FigureS3) further detailed the C-containing functional groups as: C-C/C=C (non-oxygenated ring C), C-O, C=O (carbonyl) and O-C=O (carboxylate)[48]. Similar groups were observed in LCGO thus explaining the similar hydrophilicity between LCGO-AuNR and LCGO observed above due to similar oxygenated groups[47] (see Supplementary FigureS3). The N1s spectrum of LCGO-AuNR showed the presence for C-NH and O=C-NH groups resulting from the conjugation with AuNR (see Supplementary Table1 and Supplementary FigureS3). The presence of AuNR at the outermost part of the LCGO-AuNR surface (see Supplementary Table1 and Supplementary FigureS3) ensures direct contact between the gold nanorods and the cell membrane for optical stimulation *via* photothermal effect.

Electrochemical characterisation

The cyclic voltammogram (CV) of LCGO-AuNR deposited on gold mylar electrode (LCGO-AuNR/Gold Mylar) presented a higher current and CV area than bare gold mylar (Figure6a,

c). This suggested that the LCGO-AuNR electrode interface is electroactive and charge delivery can occur by capacitive process during electrical cell stimulation.[49] However, compared to other graphene-based films, the current magnitude was relatively low mainly due to the low intrinsic conductivity of the LCGO component of the nanocomposite given that it was not reduced.[50] LCGO-AuNR/Gold Mylar shows two oxidation peaks (I' and II') which were both reversible as shown by the presence of corresponding reduction peaks III' and IV' respectively.[51] Redox peaks at similar potential values (I, II, III and IV) were observed in LCGO (Figure6b). Although they were more prominent in LCGO than in LCGO-AuNR, likely due to more effective surface electron transfer, these similar redox peaks showed conservation of reversible electrochemical properties of LCGO component after the conjugation. The functional groups associated with these redox peaks are carboxyl, phenol and quinone groups. The maintenance of the CV profile shape for 5 cycles in LCGO-AuNR/Gold mylar showed the electrochemical stability of the interface[49] (Figure6c).

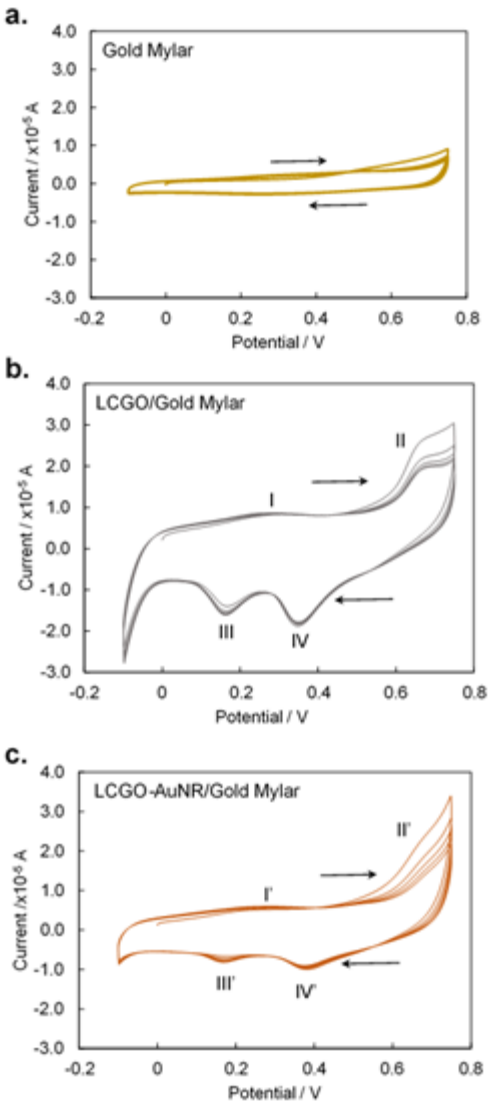

Figure 6 Cyclic voltammogram of **a.** bare gold mylar electrode, **b.** LCGO on gold mylar electrode (LCGO/Gold Mylar) and **c.** LCGO-AuNR on gold mylar electrode (LCGO-AuNR/Gold Mylar). Arrows show the scanning direction. I, II, III and IV indicate redox peaks on LCGO/Gold Mylar. The corresponding peaks on LCGO-AuNR/Gold Mylar are labelled I', II', III' and IV'. CV of each electrode was measured for 5 cycles as shown here.

Biocompatibility

Cell adhesion on LCGO-AuNR films

The cell adhesion studies showed that LCGO-AuNR films supported NG108-15 cell adhesion with 70.2±7.6% of cells attached at 4h *(n=6)* (Figure7a). The number of cells attached to LCGO-AuNR remained statistically similar over the 24h period (*n=6*, one-way ANOVA, *p<0.05; Tukey HSD; p>0.05*). Furthermore, the cell adhesion properties and cytotoxicity observed on LCGO-AuNR films *(n=6)* showed no difference compared to standard tissue culture plastic (TCP) *(n=5-6)* (one-way ANOVA, *p<0.05; Tukey HSD; p>0.05*). This suggested that the LCGO-AuNR surface allowed the cells to undergo the normal process of cell attachment[52] despite the observed lower cell adhesion compared to LCGO films at 24h. This could be explained by the difference in cytotoxicity observed between the two films at 24h (Figure7c) (*(n=6) LCGO at 24h; (n=6) LCGO-AuNR at 24h;* one-way ANOVA, $p<0.05$; Tukey HSD, $p<0.05$).

The analysis of surface area occupied by the cells showed a steady increase over 24h on LCGO-AuNR films *(n=561-1136 cells)* at levels similar to air-plasma treated glass (control) *(n=524-1318 cells)* (one-way ANOVA, $p< 0.05$; Tukey HSD, $p< 0.05$) (Figure7b). Initially, NG108-15 cells were spherical in shape at 4h. Flattening of cells and formation of extensions were observed over the 24h period (see Supplementary FigureS4). This phenomenon translates into the process of cell spreading normally observed during cell adhesion due to creation of focal adhesion points.[53] Such process is essential for future cell development such as proliferation and differentiation. At 8h and 24h, the mean cell area occupied by NG108-15 cells was, however, lower on LCGO-AuNR films compared to

LCGO which may imply better cell adhesion on LCGO films (LCGO-AuNR at 8h, *n=1136 cells*; LCGO-AuNR at 24h, *n=876 cells*; LCGO at 8h, *n=705*; LCGO at 24h, *n=566 cells*; one-way ANOVA, $p<0.05$; Tukey HSD, $p< 0.05$).

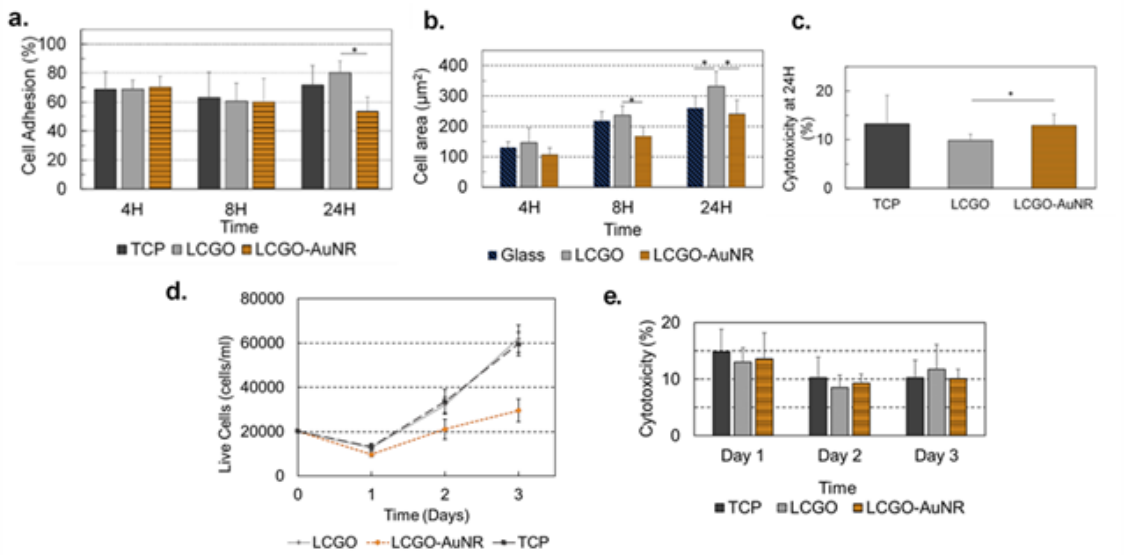

Figure 7 a. Cell adhesion on tissue culture plastic (TCP) (*n=6*), LCGO films (*n=6*) and LCGO-AuNR films (*n=6*) over 24h. The number of cells adhered is expressed as a percentage of the total number of cells present at each time point b. Evolution of cell area of NG108-15 cells cultured on glass substrate, LCGO films and LCGO-AuNR films. Number of cells analysed per condition, *n=419-1318* c. Cytotoxicity of TCP (*n=6*), LCGO films (*n=6*) and LCGO-AuNR films (*n=6*) at 24h. d. Cell proliferation profile of NG108-15 cells cultured on LCGO films, LCGO-AuNR films and TCP over 3 days. e. Cytotoxicity on NG108-15 cells cultured on TCP, LCGO films and LCGO-AuNR films over a period of 3 days. Note: Mean values are represented in Figures 7a-e. Error bars represent the standard deviation, S.D. "*" indicates a statistically significant difference of p-value, $p< 0.05$ (one-way ANOVA and Tukey HSD post-hoc test).

Cell Proliferation on LCGO-AuNR films

NG108-15 cells showed a steady increase in cell number on LCGO-AuNR films at a proliferation rate of 0.47±0.08 *(n=6)* (see Figure7d and Supplementary Table 2). Thus, LCGO-AuNR films supported cell proliferation. The rate of cell proliferation observed on LCGO-AuNR films was lower compared to that of LCGO films and TCP (see Supplementary Table 2). However, a statistical difference was only shown between LCGO-AuNR and LCGO (LCGO-AuNR, $n=6$; LCGO, $n=5$; one-way ANOVA, $p<0.05$; Tukey HSD, $p<0.05$). A Univariate Analysis of Variance (Interaction Analysis) indicated that the difference in cell number observed at the different time points is dependent on differences in material type ($n=5$-6, for each substrate per time point; Univariate Analysis of Variance (Interaction Analysis), $p<0.05$). Consequently, this difference in cell number may be due to the presence of AuNR as their possible effect on cell proliferation has previously been reported.[54] An initial drop in cell number was noted on all three surfaces possibly due to seeding and inherent cytotoxicity of the surfaces (Figure7d).

Furthermore, NG108-15 expressed similar cytotoxicity on LCGO-AuNR films (n= compared to LCGO and TCP over the 3-day period (Figure7e) (one-way ANOVA, $p<0.05$; Tukey HSD, $p>0.05$). This confirms that the lower proliferation rate of NG108-15 cells observed on LCGO-AuNR is not primarily due to the cytotoxicity measured at these time points but due to direct material effect on proliferation.

Cell Differentiation on LCGO-AuNR films

NG108-15 cells were able to differentiate on the LCGO-AuNR films and presented fine neurites (Figure8a). The neurites stained for βIII-tubulin (green) which is a protein involved in neurogenesis and expressed in NG108-15 cells.[35] The percentage of cells expressing neurites on LCGO-AuNR films steadily increased from 4.1% on Day 0 to 71% on Day 7 of differentiation (Figure8b) (*n=291-484*; one-way ANOVA, $p<0.05$; Tukey HSD, $p<0.05$). At Day 7, the number of differentiating NG108-15 cells was statistically superior on LCGO-AuNR films *(n=484)* compared to LCGO films *(n=625)* and glass *(n=742)* (one-way ANOVA, $p<0.05$; Tukey HSD, $p<0.05$) (Figure8b). The number of neurites per cell was also assessed for each condition (Figure8 c, d, e). Considering the differentiating cells on LCGO-AuNR films, the proportion of cells presenting two neurites and three or more neurites increased from 25% to 52% and 0% to 33% respectively over the 7-days differentiation period. A Pearson Chi-square test showed that this change in distribution over the 7-day differentiation period was statistically significant thus confirming the differentiation process (*n=291-484*; Pearson Chi-square; $p< 0.05$). Similar trend was observed on the controls (LCGO, *n=354-625*; Glass, *n=329-742*; Pearson Chi-square; $p< 0.05$) (Figure 8 d and e). Hence, NG108-15 cells mostly adopted a bipolar or multipolar morphology. This denotes normal differentiation of the cell line on LCGO-AuNR films as NG108-15 cells are models for development and differentiation of cholinergic peripheral neurons (including motor neurons) which have this morphology.[55,56] Moreover, the proportion of cells expressing one, two, three or more neurites on Day 3 *(n= 434)* and Day 7 *(n=484)* on LCGO-AuNR films were statistically different compared to the controls (Pearson Chi-

square; $p<0.05$), with LCGO-AuNR films showing a higher proportion of cells expressing two or more neurites (85%) on Day 7 (Figure 8c).

Conclusions

A liquid crystal graphene oxide-gold nanorods (LCGO-AuNR) nanocomposite was successfully fabricated by covalently conjugating liquid crystal graphene oxide (LCGO) and protein-coated gold nanorods (AuNR) *via* EDC/NHS chemistry. The nanocomposite presented photoactivity in the NIR range by expressing a localized surface plasmon resonance peak at 798nm due to the gold nanorods. Our results further demonstrate the electroactive capacitive properties of the LCGO-AuNR electrode coating thus showing its suitability as an interface for near-infrared and electrical cell co-stimulation. The LCGO-AuNR coating further presented a wrinkled morphology with adequate density of gold nanorods, thereby offering a large effective surface area for electrical cell stimulation and effective optical stimulation. It showed good biocompatibility, in terms of cell viability, adhesion, proliferation and differentiation of NG108-15 neuronal cells on LCGO-AuNR films under passive culture conditions. Thus, these results confirmed its promising potential as an electrode-tissue interface for electrical and NP-NIR co-stimulation of neuronal cells in future studies.

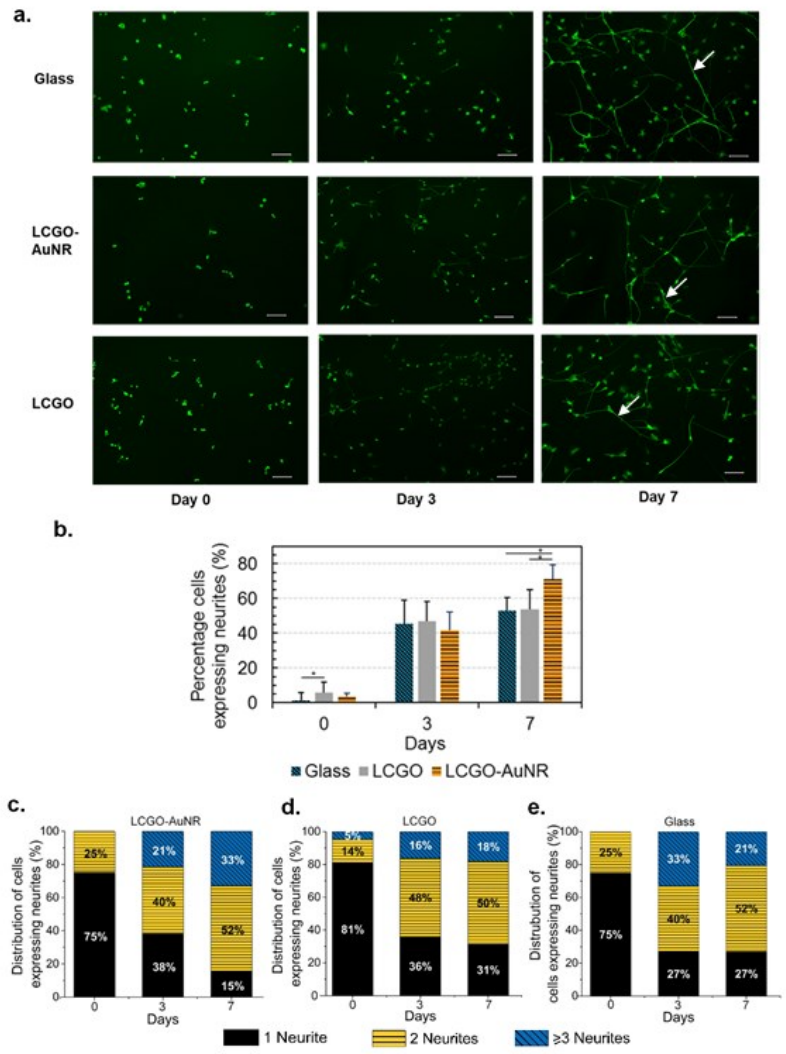

Figure 8 a. Differentiation of NG108-15 cells on glass, LCGO-AuNR films and LCGO films over a 7-day period. Pictures were taken at Day 0, 3 and 7 of differentiation. Scale: 100µm; 10X magnification. Over the 7-day period, neurite outgrowth was observed (see arrows). Cells were stained for βIII–tubulin (green). Cell extensions observed were considered as neurites *if* ≥1X cell body in length. b. Percentage number of NG108-15 cells expressing neurites on glass *(n=329-742)*, LCGO films *(n=354-625)* and LCGO-AuNR films *(n=291-484)* at Day 0, 3 and 7 of differentiation. The percentage cells expressing neurites increased steadily over the 7-day period for all three surfaces with LCGO-AuNR presenting highest percentage of differentiating

cells at Day 7. Distribution of number of neurites per differentiating cell on c. LCGO-AuNR films, d. LCGO films and e. glass at day 0, 3 and 7 of differentiation. The percentage number of NG108-15 cells expressing three or more neurites at Day 7 was highest on LCGO-AuNR films at 33%. Note: Mean values are represented in Figures 8b. Error bars represent the standard deviation, S.D. "*" indicates a statistically significant difference of p-value, $p< 0.05$ (one-way ANOVA and Tukey HSD post-hoc test).

Methods

Synthesis of liquid crystal graphene oxide-gold nanorods nanocomposite (LCGO-AuNR)

Our fabrication method was derived from Yang *et al*. (2012) and Liu *et al.* (2016).[57,58] 10 ml of 1 mg ml^{-1} liquid crystal graphene oxide aqueous suspension (LCGO) (ANFF, University of Wollongong, Australia) was sonicated for 2h. Then, EDC/NHSS solution (5ml) and 2-(N-morpholino) ethanesulfonic acid (MES) buffer (500 mM; 5 ml) at pH 6.1 (Sigma-Aldrich Pty Ltd, Australia) were added. The EDC/NHSS solution consisted of N-(3-Dimethylaminopropyl)-N′-ethylcarbodiimide hydrochloride (EDC) (40 mM) and N-Hydroxysulfosuccinimide sodium salt (NHSS) (20 mM) (Sigma-Aldrich Pty Ltd, Australia). The LCGO-EDC/NHSS solution was stirred at room temperature for 1h to form activated LCGO (a-LCGO) which was then washed by repeated centrifugation and resuspension in MES buffer (50 mM) at pH 6.1. a-LCGO was recovered by centrifugation and re-dispersed in MES buffer (10 ml; 50 mM) at pH 6.1. Protein-coated gold nanorods

solution (AuNR) (10 ml; 0.039 mg ml^{-1}) was prepared by diluting stock AuNR (3.9 mg ml^{-1}; $5.2x10^{12}$ nanoparticles ml^{-1}; Nanopartz Inc., USA) in MES buffer (50 mM) at pH 6.1. The AuNR solution (10 ml; 0.039 mg ml^{-1}) was added to a-LCGO solution. The mixture was stirred overnight at 150rpm at 20°C (avoid light). The LCGO-AuNR aqueous suspension obtained was purified by dialysis (dialysis membrane cut-off of 14kDa; Sigma-Aldrich Pty Ltd, Australia) in MilliQ water (18MΩ.cm at 25°C) at 4°C for 4 days. Dialysis water was changed 3 times *per* day. After the dialysis, the LCGO-AuNR suspension was recovered and stored at 4°C.

Fabrication of LCGO-AuNR coated electrodes

LCGO-AuNR films were formed on gold mylar conductive substrate (ANFF University of Wollongong, Australia) for electrode fabrication. Firstly, gold mylar was air-plasma treated at a flow rate of 2 sccm for 20min at 50W. The air-plasma apparatus was composed of a plasma reactor connected to an RF generator (Model RFG100/13) and a manual impedance matching network (MMN150) from Coaxial Power Systems Ltd, UK. LCGO-AuNR films were formed using drop-casting technique. LCGO-AuNR suspension (171 µl; 0.234 mg ml^{-1}) was deposited per cm^2 of gold mylar and air-dried for 24h in sterile condition. This was repeated 3 times to form a 3-layer thick film of LCGO-AuNR films (0.12mg cm^{-2}). LCGO-AuNR films on glass coverslips were made similarly for *in vitro* testing. Control LCGO films on glass coverslips and on gold mylar were also made *via* this method.

Material characterisation and topography

Fourier transform infrared spectroscopy (FTIR) (NicoletiS5 FT-IR Spectrometer, Thermo Scientific) was performed on LCGO-AuNR and LCGO solid samples. Samples were prepared by freeze-drying aqueous suspensions of LCGO-AuNR (0.234 mg ml^{-1}) and LCGO (1 mg ml^{-1}) for 24h (FreeZone Benchtop Freeze Dry System, Labconco). AuNR solid samples were made by air-drying drop-casted AuNR suspension (0.039 mg ml^{-1}). UV-Vis spectrophotometry (Cary50Bio UV-Visible spectrophotometer, Varian Instruments) of LCGO-AuNR suspension was performed in a quartz cuvette. The UV-Vis spectrum was used to calculate the concentration of LCGO-AuNR suspension using Beer's Law:

$$A_{230nm} = c_{LCGO} d \varepsilon_{LCGO} \quad (2) \qquad A_{798nm} = c_{AuNR} d \varepsilon_{AuNR} \quad (3)$$

where A_{230nm} is the absorbance at 230nm, c_{LCGO} is the concentration of LCGO (mg ml^{-1}), d is the path length of the cuvette (1 cm), ε_{LCGO} is the extinction coefficient of LCGO (53ml.mg^{-1}.cm^{-1}),[59] A_{798nm} is the absorbance at 798 nm, c_{AuNR} is the concentration of AuNR (mg ml^{-1}) and ε_{AuNR} is the extinction coefficient of AuNR (19.7ml.mg^{-1}.cm^{-1}). Summation of the amount of LCGO and AuNR in 1ml of suspension provides the concentration of LCGO-AuNR produced in mg ml^{-1} *(n=4)*. UV-Vis spectrophotometry of LCGO aqueous suspension and AuNR aqueous solution was also performed. Amount of LCGO-AuNR suspension produced at each production cycle was measured using graduated cylinder *(n=3).*

Scanning Electron Microscopy (SEM) (ZEISS Supra40VPSEM, Carl Zeiss Pty Ltd) was performed on single-layer LCGO-AuNR films. LCGO-AuNR suspension was drop-cast onto a

silicon wafer and dried in air for 24h in sterile conditions. LCGO and AuNR samples were prepared similarly. SEM images at 50000X magnification were further used to determine the density of gold nanorods on the single-layer LCGO-AuNR film. The area of SEM images (50000X; *n=3*) of LCGO-AuNR films was measured and the number of gold nanoparticles present were counted. The density of gold nanoparticles, D, present was determined via Equation (1).

$$D = \frac{Number\ of\ gold\ nanorods\ present}{Surface\ area\ of\ LCGO{-}AuNR\ film} \quad (1)$$

LCGO-AuNR single-sheets were observed using transmission electron microscopy (TEM) (JEOL JEM-1010 Electron Microscope, JEOL Ltd.) at an accelerating voltage of 100kV. LCGO-AuNR samples were prepared by placing 2 µl of 0.2 mg ml^{-1} suspension on soft carbon grids and air-drying. Control LCGO samples were prepared by placing soft carbon grids on a 15 µl drop of LCGO suspension (0.2 mg ml^{-1}) for 10 min and air-drying.

Surface properties

Atomic force microscopy (AFM) (MultiMode 8-HR, Bruker) was performed in tapping mode and at a scanning rate of 0.996Hz on LCGO-AuNR films on gold mylar *(n=3)* and on glass substrate *(n=3)* at (0.12 mg cm^{-2}). Height mode AFM images of the surface (5µm x 5µm) were captured and processed in Nanoscope Analysis v1.40 to measure the surface

roughness. Static contact angle measurements were performed by sessile drop method (FTA1000 Drop Shape Instrument, FirstTen Angstroms™) on the LCGO-AuNR films (0.12mg cm^{-2}) *(n=3)* using MilliQ water (18MΩ.cm at 25°C). X-ray photoelectron spectroscopy (XPS) scans of the LCGO-AuNR (*n=3*) and LCGO films (*n=3*) were performed (AXIS Nova XPS, Kratos Analytical Shimadzu Group Company). Samples were prepared by drop-casting the LCGO and LCGO-AuNR suspension on silicon wafers and air-drying.

Electrochemical characterisation

Cyclic voltammetry (CV) of LCGO-AuNR coated gold mylar electrodes (0.12 mg cm^{-2}) was recorded at room temperature and pressure (CHI430A Electrochemical Analyser, CH Instruments, Inc.). The 3-electrode cell used consisted of a working electrode (LCGO-AuNR on gold mylar electrode), an Ag/AgCl (3.0M NaCl) reference electrode and a platinum mesh auxiliary electrode. CV measurements were recorded in phosphate buffer saline solution at pH 7.4 in the potential window of -0.1 to 0.75 V and at a scan rate of 50 mV s^{-1} for 5 cycles. Controls comprised of bare gold mylar electrodes and LCGO coated electrodes (0.12 mg cm^{-2}).

Cell culture

NG108-15 cells (ATCC) (passage 17) were used. For cell adhesion and proliferation studies on LCGO-AuNR films, NG108-15 cells were cultured in cell proliferation media (DMEM + 10%FBS + 1%L-glutamine + 1%Penicillin/Streptomycin) (Sigma-Aldrich Pty Ltd, Australia) under standard tissue culture conditions (5%CO_2 and at 37°C). For cell differentiation

studies on LCGO-AuNR films, NG108-15 cells were cultured in differentiation media (DMEM + 1%FBS + 1%L-glutamine + 1%Penicillin/Streptomycin) (Sigma-Aldrich Pty Ltd, Australia) in 5%CO_2 and at 37°C. All films and surfaces were sterilised using 70% ethanol followed by rinsing with sterile MilliQ water prior to cell seeding.

Cell adhesion and cytotoxicity studies

Polystyrene 96-well tissue culture plates (Corning®) (TCP) were coated with 3-layer thick LCGO-AuNR films (0.12 mg cm^{-2}) made by repeated drop-casting and air-drying. Controls included LCGO films prepared similarly and as-received (TCP). NG108-15 cells were seeded on each substrate at a density of $8x10^4$cells ml^{-1} (100 µl per well) and were incubated for 4h, 8h and 24h in 5%CO_2 and at 37°C. Number of adhered cells to each substrate at each time point was estimated by lactate dehydrogenase (LDH) assay (CytoTox96 assay Kit, Promega) and was expressed as a percentage of the total number of cells present (*n=5-6 wells per conditions*). CytoTox96 assay Kit was also used to determine cell cytotoxicity at 24h by measuring the LDH released by dead cells into the culture media (*n=6 wells per conditions*).

To measure cell area, LCGO-AuNR films on glass coverslips (0.12 mg cm^{-2}), were seeded with NG108-15 cells at $8x10^4$cells ml^{-1}. Cells were incubated for 4h, 8h and 24h. At each time point, coverslips with the adhered cells were fixed and stained for βIII-tubulin (*see below*). Pictures of cells were taken *via* fluorescence microscopy (Olympus IX70 Fluorescence Microscope and SPOT RT230 Slider Scientific Digital Camera System). Controls included air-plasma treated glass coverslips and LCGO films on glass coverslips

(0.12 mg cm^{-2}). Then the cell area was calculated for 400 cells minimum per condition using ImageJ (*n=419-1318).*

Cell proliferation and cytotoxicity studies

NG108-15 cells were seeded at a density of $2x10^4$ cells ml^{-1} (100µl per well) on LCGO-AuNR films (0.12 mg cm^{-2}) prepared in standard 96-well TCP(Corning®) by drop-casting and air-drying. Cells were incubated at 5% CO_2 and 37°C for 3 days. Number of cells present at 1, 2 and 3 days in each well *(n=6)* was determined using LDH assay (CytoTox96 assay Kit, Promega). The cell proliferation rate was calculated by Equation (4):

$$P = \log(ND3) - \log(ND1) \quad (4)^{[60]}$$

where *P* is the rate of cell proliferation, *ND1* is the cell density (cells ml^{-1}) at day1 and *ND3* (cells ml^{-1}) is the cell density at day3.[60] The cytotoxicity at each time point was determined using LDH assay (CytoTox96 assay Kit, Promega) and expressed as a percentage of the total cells present. Controls included as-received TCP *(n=6)* and LCGO films *(n=5-6)* prepared similarly to LCGO-AuNR films for both proliferation and cytotoxicity studies.

Cell differentiation studies

NG108-15 cells in proliferation media were seeded at $3x10^4$ cells ml^{-1} on LCGO-AuNR films on glass coverslips (0.12 mg m^{-2}) and were incubated for 24h. The media was then replaced with differentiation media and cells were incubated for 0, 3 and 7 days. At each

time point, cells were stained for βIII-tubulin *via* indirect immunofluorescent staining (*see below*) and observed *via* fluorescence microscopy (Olympus IX70 Fluorescence Microscope and SPOT RT230 Slider Scientific Digital Camera System). For each time point, cells differentiated on LCGO-AuNR films *(n=291-484)* were analysed on ImageJ to count the number of neurites *per* cell. A neurite was defined as an extension ≥1X diameter of the cell body. The number of cells presenting neurites were expressed as a percentage of the total number of cells counted at each time point. Controls included cells differentiated on air-plasma treated glass coverslips *(n=329-742)* and LCGO films on glass coverslips *(n=354-625)*.

Immunofluorescence staining of NG108-15 cells

NG108-15 cells were fixed in 10% neutral buffered formalin (NBF) for 20min. NBF was removed and cells were conserved in 1X phosphate buffer saline solution (1XPBS) at 4°C for 24h. Cells were permeabilised by incubation in 10% goat serum with 0.1% TritonX100 for 1h. Cells were then washed in 1XPBS solution and primary antibody (1/1000 purified mouse antibody monoβ-tubulin (TUJ1) Covance® + 10% goat serum + 0.1% TritonX100) was added. Cells were incubated for 2h at room temperature and washed in 1XPBS. The secondary antibody (1/2000 Alexa Fluor® 488 goat anti-mouse IgG, Invitrogen® + 10% goat serum + 0.1% TritonX100) was added and cells were incubated for 2h. Cells were washed in 1XPBS and mounted on microscope slides.

Statistical Analysis

All experiments were performed at least in triplicate. Results were reported as mean ± standard deviation (mean ± S.D.). Microsoft Office Excel, OriginPro2015 and IBM™ SPSS™ Statistics25 were used for statistical analysis. One-way analysis of variance (ANOVA) and Tukey's HSD (Post-hoc) tests were performed for statistical comparisons namely in surface roughness, contact angle, cell adhesion, cell proliferation and cell differentiation studies. Two-tailed *t*-test was also performed on XPS results for statistical comparison. For ANOVA, Tuckey's HSD and *t*-tests, a statistically significant difference was established for $p<0.05$. A Univariate Analysis of Variance (Interaction Analysis) was further performed in cell proliferation studies to evaluate the dependence of the effect observed, on the materials assessed. Statistical significance was established for $p<0.05$. A Pearson Chi-square test was performed in the cell differentiation studies for statistical comparison of cell distributions. A statistically significant difference was established for $p<0.05$.

Data Availability Statement

The data generated and analyzed during the current study are available in the Supplementary Information files and in the figshare repository, https://figshare.com/s/2330ac2ce5fa31d9cca4

Acknowledgements

This work was supported by Swinburne University of Technology, the ARC Centre of Excellence for Electromaterials Science (ACES) [CE140100012], the ARC Training Centre in Biodevices [IC140100023] and the Australian Research Council Centre of Excellence Scheme. This work was performed in part at the ANFF - Vic Biointerface Engineering Hub (Swinburne University of Technology) and the Materials Node (University of Wollongong) of the Australian National Fabrication Facility (ANFF). A company established under the National Collaborative Research Infrastructure Strategy to provide nano and microfabrication facilities for Australia's researchers. The authors further acknowledge the facilities, the scientific and technical assistance of the RMIT University's Microscopy & Microanalysis Facility, a linked laboratory of the Australian Microscopy & Microanalysis Research Facility. The authors also thank Biofab3D@ACMD - St Vincent's Hospital for their support.

References

[1] M. C. Ford, O. Alexandrova, L. Cossell, A. Stange-Marten, J. Sinclair, C. Kopp-Scheinpflug, M. Pecka, D. Attwell, B. Grothe, *Nat. Commun.* **2015**, *6*, 8073.

[2] E. Stewart, N. R. Kobayashi, M. J. Higgins, A. Quigley, S. S. Jamali, *Tissue Eng. Part C Methods* **2015**, *21*, 385.

[3] K. H. Lee, C. D. Blaha, B. T. Harris, S. Cooper, F. L. Hitti, J. C. Leiter, D. W. Roberts, U. Kim, *Eur. J. Neurosci.* **2006**, *23*, 1005.

[4] R. Chen, A. Canales, P. Anikeeva, *Nat. Rev. Mater.* **2017**, *2*, 16093.

[5] S. F. Cogan, P. R. Troyk, J. Ehrlich, T. D. Plante, *IEEE Trans. Biomed. Eng.* **2005**, *52*, 1612.

[6] G. Shi, Z. Zhang, M. Rouabhia, *Biomaterials* **2008**, *29*, 3792.

[7] A. Mazzatenta, M. Giugliano, S. Campidelli, L. Gambazzi, L. Businaro, H. Markram, M. Prato, L. Ballerini, *J. Neurosci.* **2007**, *27*, 6931.

[8] A. T. Young, N. Cornwell, M. A. Daniele, *Adv. Funct. Mater.* **2018**, *28*, 1.

[9] M. H. Histed, V. Bonin, R. C. Reid, *Neuron* **2009**, *63*, 508.

[10] S. Venkatraman, J. Hendricks, Z. A. King, A. J. Sereno, S. Richardson-Burns, D. Martin, J. M. Carmena, *IEEE Trans. Neural Syst. Rehabil. Eng.* **2011**, *19*, 307.

[11] H.-C. Tian, J.-Q. Liu, D.-X. Wei, X.-Y. Kang, C. Zhang, J.-C. Du, B. Yang, X. Chen, H.-Y. Zhu, Y.-N. NuLi, et al., *Biomaterials* **2014**, *35*, 2120.

[12] A. C. Thompson, P. R. Stoddart, E. D. Jansen, *Curr. Mol. Imaging* **2014**, *3*, 162.

[13] O. Akhavan, E. Ghaderi, *Nanoscale* **2013**, *5*, 10316.

[14] O. Akhavan, E. Ghaderi, **n.d.**, DOI 10.1039/c3tb21085e.

[15] J. Wells, C. Kao, K. Mariappan, J. Albea, E. D. Jansen, P. Konrad, A. Mahadevan-Jansen, *Opt. Lett.* **2005**, *30*, 504.

[16] N. I. Smith, S. Iwanaga, T. Beppu, K. Fujita, O. Nakamura, S. Kawata, *Laser Phys. Lett.* **2006**, *3*, 154.

[17] V. Pansare, S. Hejazi, W. Faenza, R. K. Prud'homme, *Chem. Mater.* **2012**, *24*, 812.

[18] A. R. Duke, H. Lu, M. W. Jenkins, H. J. Chiel, E. D. Jansen, *J. Neural Eng.* **2012**, *9*, 036003.

[19] S. Liang, F. Yang, C. Zhou, Y. Wang, S. Li, C. K. Sun, J. L. Puglisi, D. Bers, C. Sun, J. Zheng, *Cell Biochem. Biophys.* **2009**, *53*, 33.

[20] G. Hong, S. Diao, J. Chang, A. L. Antaris, C. Chen, B. Zhang, S. Zhao, D. N. Atochin, P. L. Huang, K. I. Andreasson, et al., *Nat. Photonics* **2014**, *8*, 723.

[21] C. Paviolo, J. W. Haycock, P. J. Cadusch, S. L. McArthur, P. R. Stoddart, *J. Biophotonics* **2014**, *7*, 761.

[22] C. Paviolo, J. W. Haycock, J. Yong, A. Yu, P. R. Stoddart, S. L. McArthur, *Biotechnol. Bioeng.* **2013**, *110*, 2277.

[23] J. Yong, K. Needham, W. G. A. Brown, B. A. Nayagam, S. L. McArthur, A. Yu, P. R. Stoddart, *Adv. Healthc. Mater.* **2014**, *3*, 1862.

[24] A. R. Duke, J. M. Cayce, J. D. Malphrus, P. Konrad, A. Mahadevan-Jansen, E. D. Jansen, *J. Biomed. Opt.* **2009**, *14*, 060501.

[25] O. Akhavan, E. Ghaderi, S. A. Shirazian, *Colloids Surfaces B Biointerfaces* **2015**, *126*, 313.

[26] S. Yoo, R. Kim, J.-H. Park, Y. Nam, *ACS Nano* **2016**, *10*, 4274.

[27] R. Jalili, S. H. Aboutalebi, D. Esrafilzadeh, K. Konstantinov, J. M. Razal, S. E. Moulton, G. G. Wallace, *Mater. Horiz.* **2014**, *1*, 87.

[28] J. E. Kim, T. H. Han, S. H. Lee, J. Y. Kim, C. W. Ahn, J. M. Yun, S. O. Kim, *Angew. Chemie Int. Ed.* **2011**, *50*, 3043.

[29] N. V. Apollo, M. I. Maturana, W. Tong, D. A. X. Nayagam, M. N. Shivdasani, J. Foroughi, G. G. Wallace, S. Prawer, M. R. Ibbotson, D. J. Garrett, *Adv. Funct. Mater.* **2015**, *25*, 3551.

[30] S. Jalili-Firoozinezhad, M. H. Mohamadzadeh Moghadam, M. H. Ghanian, M. K. Ashtiani, H. Alimadadi, H. Baharvand, I. Martin, A. Scherberich, *RSC Adv.* **2017**, *7*, 39628.

[31] N. Farah, A. Zoubi, S. Matar, L. Golan, A. Marom, C. R. Butson, I. Brosh, S. Shoham, *J. Neural Eng.* **2013**, *10*, 056004.

[32] J. L. Carvalho-de-Souza, J. S. Treger, B. Dang, S. B. H. Kent, D. R. Pepperberg, F. Bezanilla, *Neuron* **2015**, *86*, 207.

[33] A. G. Tkachenko, H. Xie, Y. Liu, D. Coleman, J. Ryan, W. R. Glomm, M. K. Shipton, S. Franzen, D. L. Feldheim, *Bioconjug. Chem.* **2004**, *15*, 482.

[34] S. Link, M. A. El-Sayed, *Int. Rev. Phys. Chem.* **2000**, *19*, 409.

[35] C. Paviolo, P. Stoddart, *Nanomaterials* **2017**, *7*, 92.

[36] T. Tojima, Y. Yamane, M. Takahashi, E. Ito, *Neurosci. Res.* **2000**, *37*, 153.

[37] F. Emadi, A. Amini, A. Gholami, Y. Ghasemi, *Sci. Rep.* **2017**, *7*, 42258.

[38] J. Chen, X. Wang, T. Chen, *Nanoscale Res. Lett.* **2014**, *9*, 86.

[39] S. Su, J. Wang, E. Vargas, J. Wei, R. Martínez-Zaguilán, S. R. Sennoune, M. L. Pantoya, S. Wang, J. Chaudhuri, J. Qiu, *ACS Biomater. Sci. Eng.* **2016**, *2*, 1357.

[40] N. V. Apollo, M. I. Maturana, W. Tong, D. A. X. Nayagam, M. N. Shivdasani, J. Foroughi, G. G. Wallace, S. Prawer, M. R. Ibbotson, D. J. Garrett, *Adv. Funct. Mater.* **2015**, *25*, 3551.

[41] J. Zhang, Y. Ren, T. Xu, H. Yang, Q. Xu, *RSC Adv.* **2015**, *5*, 94809.

[42] S. Deng, V. Berry, *Mater. Today* **2016**, *19*, 197.

[43] S. Naficy, R. Jalili, S. H. Aboutalebi, R. A. Gorkin III, K. Konstantinov, P. C. Innis, G. M. Spinks, P. Poulin, G. G. Wallace, *Mater. Horiz.* **2014**, *1*, 326.

[44] J. Ma, M. Yang, F. Yu, J. Zheng, *Sci. Rep.* **2015**, *5*, 13578.

[45] D. P. Dowling, I. S. Miller, M. Ardhaoui, W. M. Gallagher, *J. Biomater. Appl.* **2011**, *26*, 327.

[46] V. Brunetti, G. Maiorano, L. Rizzello, B. Sorce, S. Sabella, R. Cingolani, P. P. Pompa, *Proc. Natl. Acad. Sci. U. S. A.* **2010**, *107*, 6264.

[47] X. Shi, H. Chang, S. Chen, C. Lai, A. Khademhosseini, H. Wu, *Adv. Funct. Mater.* **2012**, *22*, 751.

[48] N. Li, X. Zhang, Q. Song, R. Su, Q. Zhang, T. Kong, L. Liu, G. Jin, M. Tang, G. Cheng, *Biomaterials* **2011**, *32*, 9374.

[49] F. Y. Ban, S. R. Majid, N. M. Huang, H. N. Lim, *Int. J. Electrochem. Sci* **2012**, *7*, 4345.

[50] D. Zhang, X. Ouyang, J. Ma, L. Li, Y. Zhang, *Electroanalysis* **2016**, *28*, 749.

[51] A. Rose, N. Raghavan, S. Thangavel, B. U. Maheswari, D. P. Nair, G. Venugopal, *Mater. Sci. Semicond. Process.* **2015**, *31*, 281.

[52] W. Huang, B. Anvari, J. H. Torres, R. G. Lebaron, K. A. Athanasiou, *J. Orthop. Res.* **2003**, *21*, 88.

[53] S. Hong, E. Ergezen, R. Lec, K. A. Barbee, *Biomaterials* **2006**, *27*, 5813.

[54] S. Gioria, J. Lobo Vicente, P. Barboro, R. La Spina, G. Tomasi, P. Urbán, A. Kinsner-Ovaskainen, R. François, H. Chassaigne, *Nanotoxicology* **2016**, *10*, 736.

[55] T. Tojima, Y. Yamane, M. Takahashi, E. Ito, *Neurosci. Res.* **2000**, *37*, 153.

[56] T. Fukazawa, M. Matsumoto, T. Imura, E. Khalesi, T. Kajiume, Y. Kawahara, K. Tanimoto, L. Yuge, *Neurosci. Lett.* **2013**, *545*, 29.

[57] T. Yang, L. Liu, J. Liu, M.-L. Chen, J.-H. Wang, *J. Mater. Chem.* **2012**, *22*, 21909.

[58] L. Liu, N. Xia, J. Yu, *Microchim. Acta* **2016**, *183*, 265.

[59] G. Wang, B. Wang, J. Park, J. Yang, X. Shen, J. Yao, *Carbon N. Y.* **2009**, *47*, 68.

[60] J. M. Dubois, *Gen. Physiol. Biophys.* **2004**, 231.

Author contributions statement

D.D. performed the experiments and prepared the manuscript. S.E.M. assisted in the cyclic voltammetry measurements. A.F.Q. assisted in performing the cell culture and biocompatibility experiments. M.B.M performed the transmission electron microscopy (TEM). P.R.S., R.M.I.K., A.F.Q. and S.E.M. reviewed and assisted in the preparation of the manuscript. P.R.S., R.M.I.K., S.L.M. and S.E.M. supervised and participated in the conception of the project.

Additional information

Conflict of interest

The authors declare no conflict of interest.

Table of Contents

Summary

Today, electrical and optical neuronal cell stimulation techniques require high precision and energy efficiency respectively. As a solution, an electrode-tissue interface made of liquid crystal graphene oxide-gold nanorods composite was constructed for electrical and near infrared (NIR) co-stimulation of neuronal cells. Its photoactivity in the near-infrared range, electroactivity and biocompatibility with neuronal cells showed its promising potential for this application.

Figure

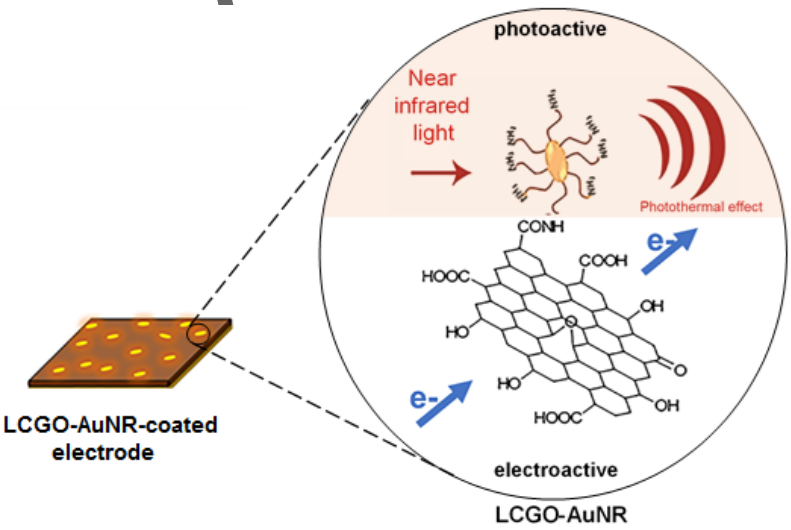

Keywords

Liquid crystal graphene oxide, gold nanorods, electrical stimulation and near-infrared stimulation, neurons